ORIGINAL ARTICLE

Model test of failure modes of high embankment and aseismic measures for buried strike-slip fault movement

Changwei Yang[1] · Jianjing Zhang[1] · Zhengzheng Wang[2] · Jiaqing Hou[1] · Changliang Si[1]

Abstract
In this article, a series of model tests for a scaled high embankment, which is located at the Yun Gui railway, have been carried out. The purpose of the model tests was to ascertain failure modes of high embankments and the efficiency of the aseismic measures for buried strike-slip fault movement. The results show: (1) failure mode of the high embankment for buried strike-slip fault movement is the tensile failure. (2) The model with CFG pile foundation, sand blanket and geogrid has the best aseismic effect, followed by the model with sand blanket and geogrid. When dislocation displacement is small, the sand blanket under the embankment can achieve better aseismic efficiency, but when the dislocation displacement is large, the sand blanket under the embankment may lose its aseismic efficiency and may cause an adverse effect on the embankment.

Keywords Strike-slip faults · Embankment · Aseismic measures · Failure mode

Introduction

Earthquakes are serious natural disasters, and the damage caused by fault dislocation on linear structures, such as a railway roadbed crossing faults and pipelines, is the most serious (Bird and Bommer 2004; Prestininzi and Romeo 2000; Yang et al. 2018).

In the western area of China, earthquake activity is high, and active faults and ground fractures are well developed. Construction of railways and highways is facing the threat of active faults and ground fractures. Formerly, a lot of work

about the impacts of active faults on constructions have been done, for example, engineering geology classification of active faults (Liu 1987), mechanical characteristics and failure modes of tunnels on active fault zones (Liu and Liu 2003; Wang and Yang 2007), pipelines (Zhang et al. 2001; Feng and Zhao 2001; Gou et al. 2017; Cui et al. 2017; Gou et al. 2018), bridges (Wang et al. 2009; Shi et al. 2009). For geotechnical engineering, the main focus of research is slope stability near active fault zones (Jiang et al. 2005), mechanical characteristics (Jiang et al. 2007) and extended mode of rock and earth mass on active faults (Liu 2004), and so on. Much experience on how to build constructions on active fault zones has been gathered. But until now, just a little work on the mechanism of the failure of high embankment caused by strike-slip fault and how to prohibit the embankment fail by using engineering measures has been done. It is one of the reasons that the design of high embankment on active faults is done according to experience.

In this article, a series of model tests for a scaled high embankment, which is located at Yun Gui railway, have been carried out. The purpose of the model tests was to ascertain failure modes of high embankment and efficiency of the aseismic measures for buried strike-slip fault movement. Finally, failure modes of high embankment and aseismic measures are summarized in this article.

✉ Zhengzheng Wang
   txh19950818@163.com

   Changwei Yang
   yangchangwei56@163.com

   Jianjing Zhang
   1209732335@qq.com

   Jiaqing Hou
   781510224@qq.com

   Changliang Si
   981447524@qq.com

[1] School of Civil Engineering, Key of Transportation Tunnel Engineering, Ministry of Education, Southwest Jiaotong University, Chengdu 610031, China

[2] School of Civil Engineering, Dalian University of Technology, Dalian 116024, China

Brief introduction of the model prototype

In this article, a series of model tests for a scaled high embankment have been finished. The line of the railway was represented with fill. The thickness of the fill was 22.6 m. The center of the maximum excavation was 3.1 m. The high embankment comprised two steps. The width of embankment bottom was 90 m, and the width of the top of the embankment was 13.4 m. The high of embankment was 20 m. The length of the railway was 200 m. The height of the embankment above the step was 8 m. The slope ratio was 1:1.75. The height of embankment below the step was 12 m. The width of step was 2 m. The thickness of soft soil layer, clay layer, and gravel bed under the embankment was 5, 5, and 40 m. The moving direction of strike-slip fault was perpendicular to the railway line.

Test design

Fabrication of the model

Design ratio of similitude

In this article, physical dimension's ratio of similitude was 1:150. Ratio of similitude of the friction angle and cohesion was 1:1. Mass, time, and length were taken as basic dimensions. The ratio of similitude of other physical quantity was computed using the π theorem. The results are presented in Table 1.

Based on this ratio of similitude, the model's dimensions are small; so that the step applied on the embankment could be omitted. A soft soil layer was merged into clay layer. According to the similarity relation, the thickness of clay layer and gravel bed was 7 and 27 cm. The high of embankment was then 14 cm. The bottom and top of the embankment were 60 and 9 cm. According to the restriction of the model box, the length and width of the model box were 130 and 100 cm. It is shown in Fig. 1.

According to the restriction of test materials, ratio of similitude was only met from items No. 1 to No. 8 listed in Table 1 in this test. Boundary effects were obvious due to the fact that the model box is small. So this test should be subjected to uncertainty analysis. And the qualitative analysis is left for a later study.

Model material

In this test, the bedrock of fault was made by two C40 concrete blocks with physical dimensions of 130 cm × 50 cm × 10 cm. The parameters of each soil layer were determined by soil sample tests and are listed in Table 2.

Test system

In Fig. 1, the test system is constituted by the hydraulic tank, lifting jack, model, displacement transducer, data acquisition system, and computer. In the test, one of the concrete blocks which was pushed by lifting jack moved ahead, to simulate the movement of a strike-slip fault. The level of displacement was monitored by the transducers arranged on the embankment. Data were collected by the data acquisition

Table 1 ratio of similitude constant of model

Nos.	Physical quantity	20 m embankment affinity constant
1	Physical dimension, L	150
2	Friction angle, φ	1
3	Cohesion, C	1
4	Displacement, s	150
5	Elasticity modulus, E	1
6	Poisson ratio, μ	1
7	Stress, σ	1
8	Strain, ξ	1
9	Gravel soil, γ	1/150

Table 2 Soil parameter

	Clay	Gravel soil
Gravel soil (kN/m3)	20	22
Cohesion (kPa)	40	29
Internal friction angle (°)	15	30

Fig. 1 Testing system
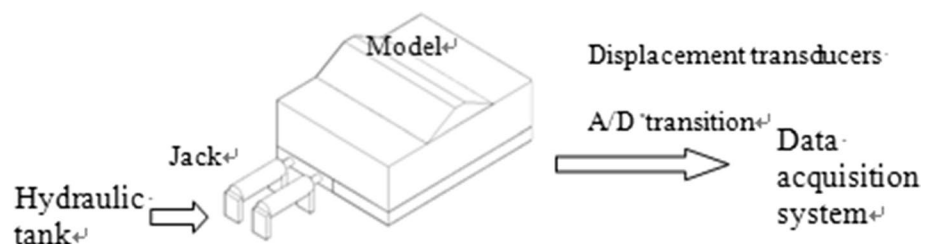
instrument and computer. There were four displacement transducers arranged in the test. Displacement transducers which were at a distance of 20 cm were located, respectively, on the two sides of top of the embankment as shown in Fig. 2. In this test, the maximum distance, maximum thrust, and speed of the lifting jack were 20 cm, 20 kn, and 1 cm/s, respectively. It was ensured that the speed of two lifting jacks was constant.

To simulating the movement of a fault, the concrete slab was pushed by the lifting jack at a speed of 1 cm/s. The deformation of the embankment was caused by the fault movement. The displacement was recorded by the displacement transducers arranged on the top of embankment, data acquisition instrument, and computer.

Test details

To ascertain failure modes of high embankment and efficiency of the aseismic measures for buried strike-slip fault movement, four models with different aseismic measures were used in the failure test. Model ① was without any aseismic measures. The thickness of coarse sand layer under the embankment in Model ② was 2 cm and expanded 10 cm along the outline of embankment bottom. Based on Model ②, bidirectional geogrid was arranged between embankment bottom and coarse sand layer in Model ③. And based on Model ③, embankment was reinforced by CFG piles which are 12 cm long and 1 cm in diameter in Model ④.

Analysis of the effect of aseismic measures

By analyzing the data collected by displacement transducers, we could compare the top displacement of the embankments between different models when the movement of strike-slip fault was an integral multiple of 10 mm. The results were depicted in Figs. 3, 4, 5, 6 and 7. In these figures, the starting point of embankment's lift side is assumed the zero. The level displacement was on the bedrock which was under the 0–50 cm embankment.

According to the above figures, these phenomena can be concluded in the process of the dislocation displacement between 0 and 30 cm. Model ① (without any aseismic measures): The level of displacement of the embankment's top was the largest. Model ② (Sand layer was put under the
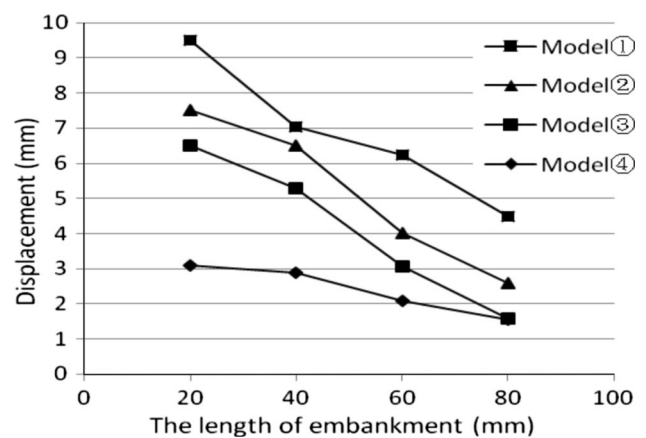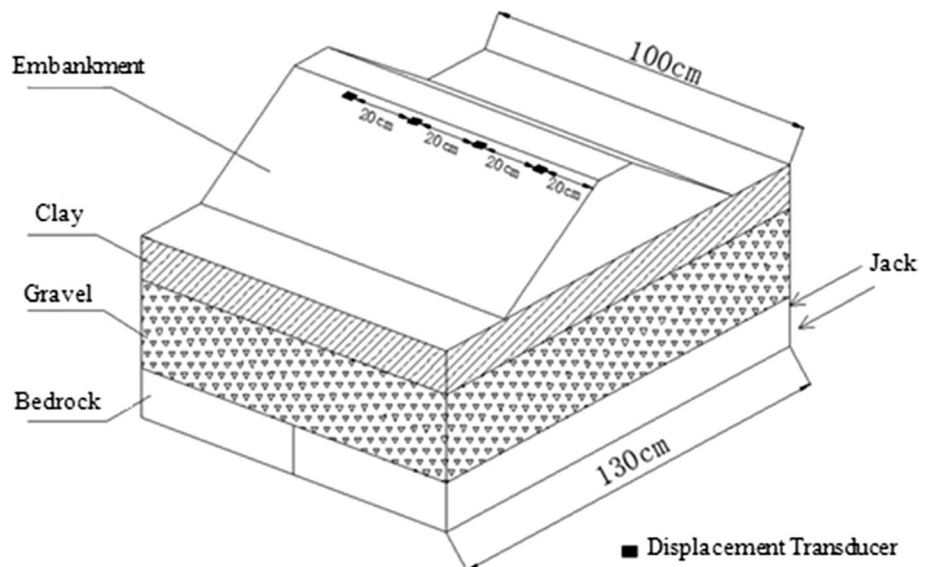

Fig. 3 Comparison of displacement on the top of embankment when dislocation displacement is 10 mm

Fig. 2 Generalized model

Fig. 4 Comparison of displacement on the top of embankment when dislocation displacement is 20 mm
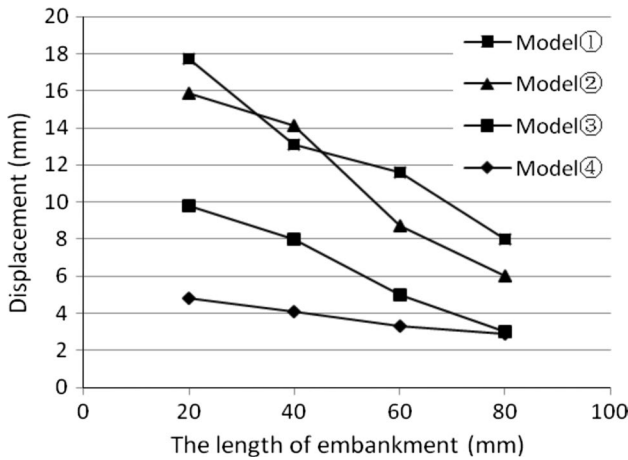

Fig. 6 Comparison of displacement on the top of embankment when dislocation displacement is 40 mm

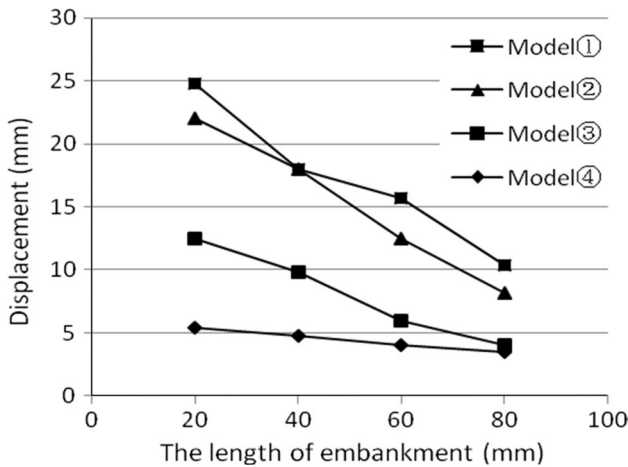**Fig. 5** Comparison of displacement on the top of embankment when dislocation displacement is 30 mm

Fig. 7 Comparison of displacement on the top of embankment when dislocation displacement is 50 mm

embankment): The level of displacement of embankment's top was the second largest. Model ③ (Sand layer and geogrid were put under the embankment): The level of displacement of embankment's top was the third largest. Model ④ (Sand layer and geogrid were put under the embankment reinforced by CFG piles): The level of displacement of embankment's top was the smallest. With the increase of strike-slip fault movement, the level of displacement of the embankment's top in Model ② was close to the displacement in Model ① gradually. When the strike-slip fault movement reached 40 mm, the level displacement of embankment's top in both Model ① and Model ② was equal. The level of displacement of the embankment's top in Model ③ was smaller than the displacement in both Model ① and Model ②. In these 4 models, the level of displacement of the embankment's top in Model ④ was the smallest. When the strike-slip fault movement was larger than 50 mm, the level displacement of
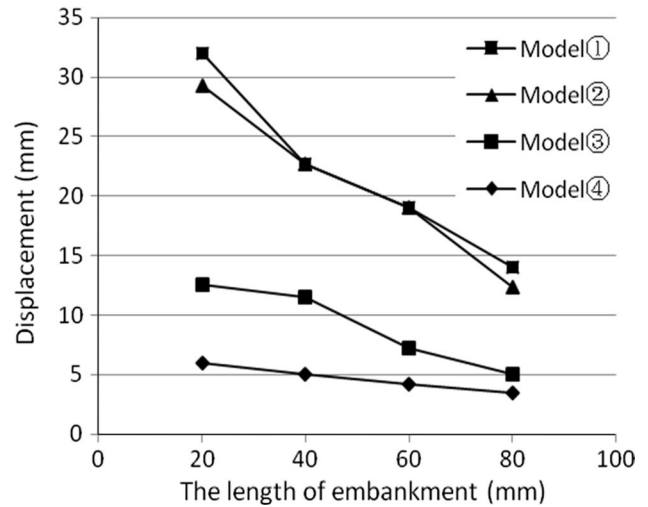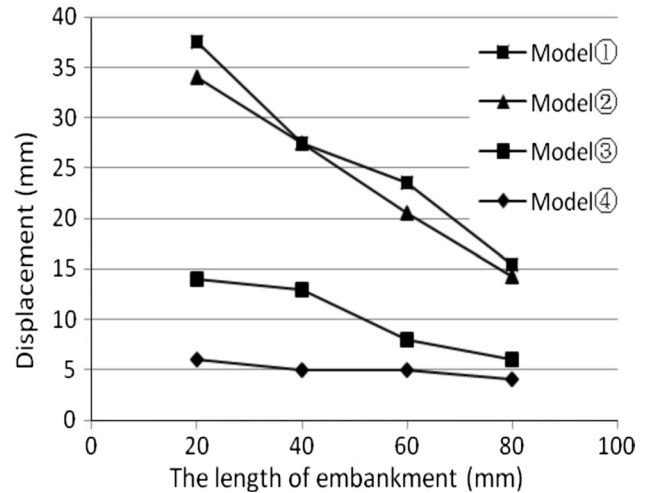
embankment's top was the largest in Model ②. The level of displacement of the embankment's top was the second largest in Model ①. The level displacement of embankment's top was the third largest in Model ③. And the level displacement of embankment's top was the smallest in Model ④.

From the test result above, these conclusions were reached. The three aseismic measures had a good effect when the strike-slip fault movement was in the process of 0–30 mm. In these three aseismic measures, putting a sand layer and a geogrid under the embankment reinforced by CFG piles had the best effect. Putting only a sand layer and a geogrid under the embankment had the second best effect. When the strike-slip fault movement was over 30 mm, putting a sand layer under the embankment had no aseismic

effect. Putting a sand layer and a geogrid under the embankment reinforced by CFG piles had the best aseismic effect (Model ④). Putting only a sand layer and a geogrid under the embankment still had the second best effect. The result of comparing these aseismic measures is summed up in Table 3. Note Displacement ratio = displacement of models with aseismic measures/that without any aseismic measures.

In order to explain the reasons for the above phenomenon, we present a preliminary analysis as follows. (1) Since the embankment was in contact with the foundation in Model ① which was without any aseismic measures, the level shearing strength caused by fault movement was easily transmitted to the top of the embankment. A greater level of displacement was generated on the top of the embankment. With the generation and extension of the plastic deformation, cracks run through the embankment. With the development of fault movement (larger than 30 mm), the transmitting of level of shear stress was prohibited by the expanding cracks in the embankment. The speed of the level movement decreases gradually. (2) Due to the cushion effect provided by the sand layer in Model ②, only a little level of shear stress was transmitted to the embankment when the fault movement was relatively small. The level of displacement of the embankment with aseismic measures was smaller than in the embankment without any aseismic measures. So cracks of the embankment in Model ② were generated later than in Model ①. With

the development of the fault movement, the speed of the level of displacement remained constant. The speed of the level displacement on the top of the embankment in Model ① was decreasing, and the speed of the level displacement of the embankment in Model ② was larger than in Model ①. (3) According to the previous test results, the friction angle between geosynthetics and padding was smaller than in the padding. Putting a sand layer and a geogrid under the embankment were equal to the decrease in the level of force transmitted to the embankment in the process of fault movement. So when the fault movement was small, the displacement on the top of the embankment decreased on the base of Model ②. (4) Due to interaction between soil and piles, the displacement on the top of the embankment of Model ④ with CFG piles in the foundation decreases on the base of Model ③.

Failure modes analysis of the embankment

With the development of fault movement, cracks generate and increase. Crack generation and failure modes were showed in Figs. 8, 9, 10, 11, 12, 13, 14 and 15.

From the Figs. 8, 9, 10, 11, 12, 13, 14 and 15, crack patterns in different models were mainly unanimous. From the lift figures of Fig. 8, 10, 12 and 14, cracks begin from

Table 3 Displacement ratio of models with aseismic measures to that without any aseismic measures

Displacements	Measuring points															
	Model ①				Model ②				Model ③				Model ④			
	Ratio				Ratio				Ratio				Ratio			
	20 cm	40 cm	60 cm	80 cm	20 cm	40 cm	60 cm	80 cm	20 cm	40 cm	60 cm	80 cm	20 cm	40 cm	60 cm	80 cm
10 mm	100%	100%	100%	100%	79%	91%	64%	57%	69%	75%	50%	36%	33%	40%	33%	33%
20 mm	100%	100%	100%	100%	89%	108%	76%	74%	55%	61%	45%	39%	26%	32%	29%	34%
30 mm	100%	100%	100%	100%	87%	102%	79%	79%	47%	53%	40%	38%	22%	25%	25%	30%
40 mm	100%	100%	100%	100%	93%	100%	100%	112%	41%	51%	38%	43%	19%	21%	22%	27%
50 mm	100%	100%	100%	100%	110%	100%	115%	113%	41%	47%	40%	42%	18%	18%	23%	28%

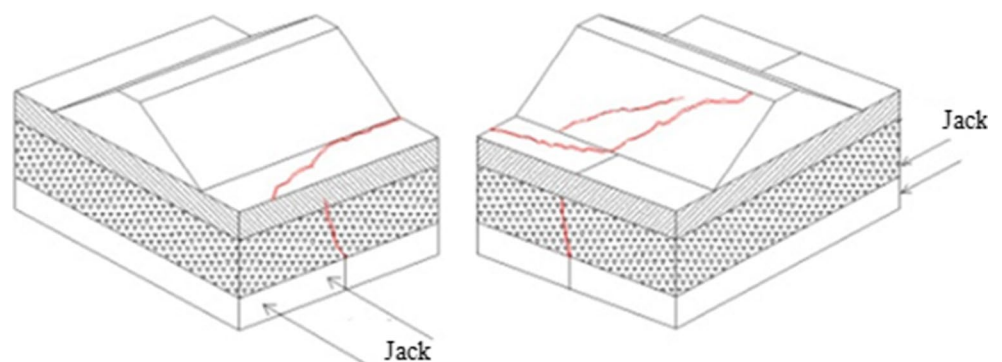

Fig. 8 Cracks of embankment in Model ①

Fig. 9 Cracks of embankment in Model ①

the boundary of a buried strike-slip fault and extend to the embankment at a 30° angle. Cracks on the embankment were mostly at a 40°–50° angle. From the right side of Figs. 8, 10, 12 and 14, cracks begin from the boundary of buried strike-slip fault and extend to the embankment at 30° angle or the embankment bottom.

When the level of displacement occurred in faults, a part of embankment was pushed by level of force transmitting up. With level of displacement of this part of embankment, the whole embankment had a bending deflection in the horizontal plane. The boundaries of two sides of the embankment were under a tensional and compressional stress condition. When movement increases, boundaries of the two sides of the embankment were be ripped. The failure of the embankment is shown in Fig. 16. According to the failure phenomenon, the failure mode of the embankment was tensile failure with buried strike-slip fault movement.
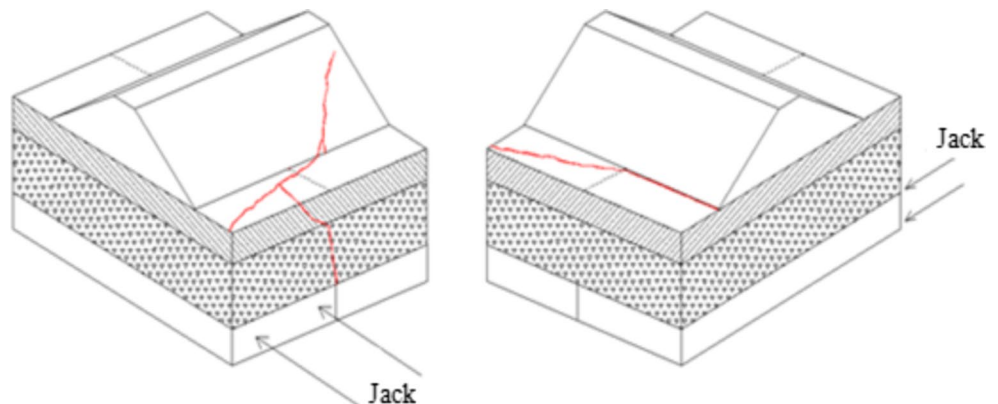
Conclusions

According to the test results above, these conclusions can be made.

1. Comparing different aseismic measures on the embankment with buried strike-slip fault movement, putting sand layer and geogrid under the embankment reinforced by CFG piles had the best aseismic effect. Putting sand layer and geogrid under the embankment had the second best aseismic effect. Only a putting sand layer under the embankment had certain aseismic effect when buried strike-slip fault movement was small. But it was mainly without any aseismic effect when buried strike-slip fault movement was large.

2. With buried strike-slip fault movement, failure mode of high embankment was mainly tensile failure. And aseismic effect depends largely on energy dissipation effect of different aseismic measures.
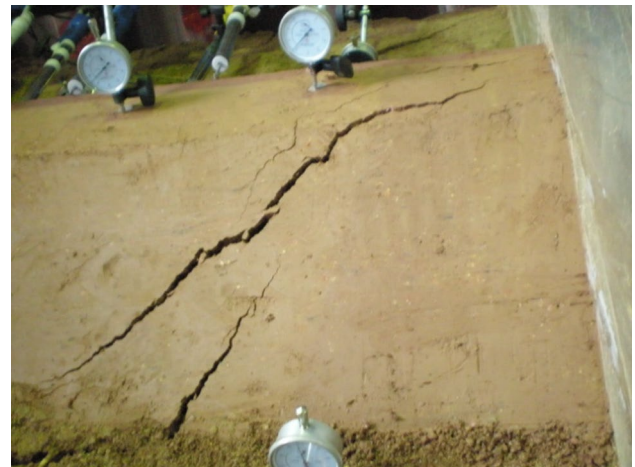

Fig. 11 Cracks of embankment in Model ②
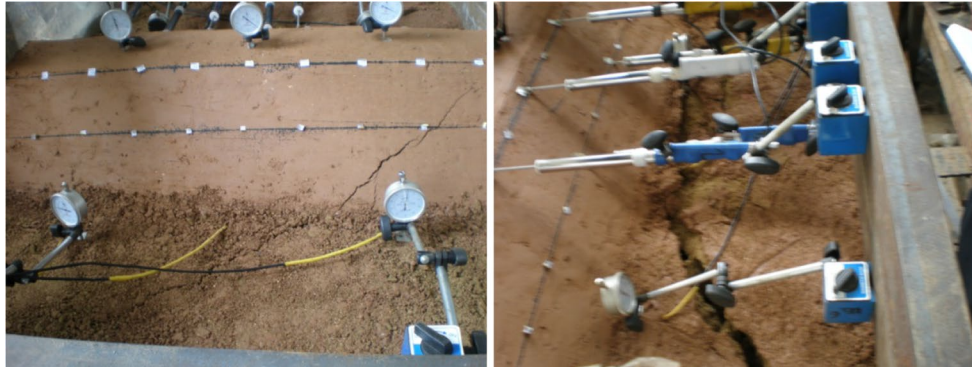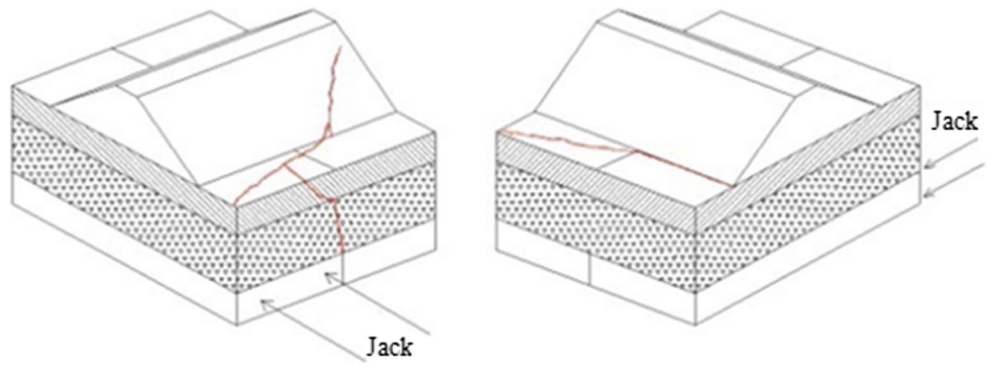
Fig. 10 Cracks of embankment in Model ②

Fig. 12 Cracks of embankment in Model ③

Fig. 13 Cracks of embankment in Model ③

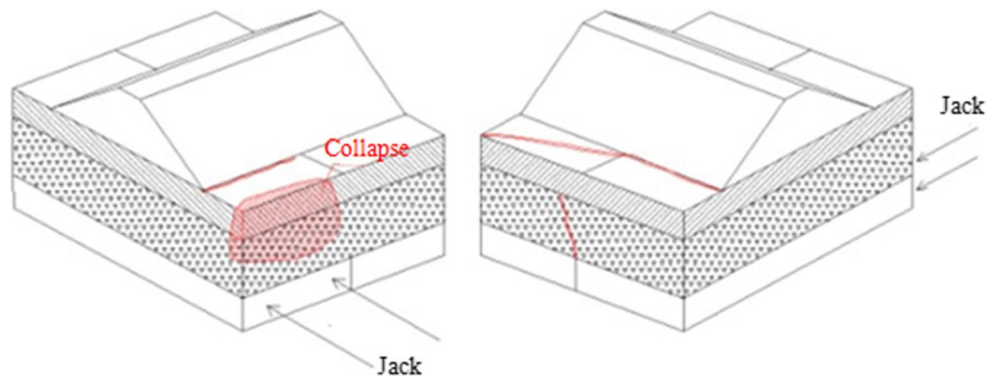**Fig. 14** Cracks of embankment in Model ④

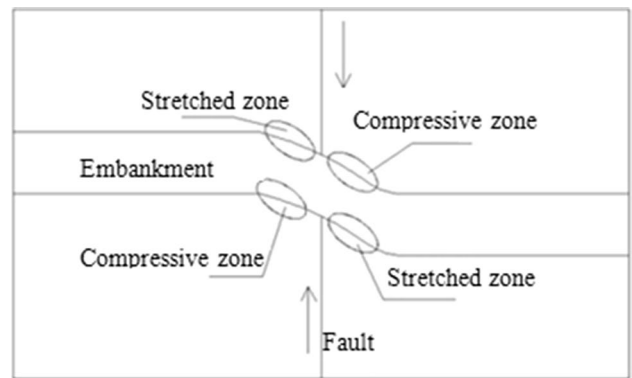**Fig. 15** Cracks of embankment in Model ④

Fig. 16 Tensile failure of embankment

3   With buried strike-slip fault movement, cracks of high embankment were not vertical and connective, but at 40–50 angle.

Compliance with ethical standards

Conflict of interest   The authors of this manuscript do not have any conflicts of interest regarding the publication of this article.

Referrence

Bird JF, Bommer JJ (2004) Earthquake losses due to ground failure. Eng Geol 75:47–179

Cui K, Yang WH, Gou HY (2017) Experimental research and finite element analysis on the dynamic characteristics of concrete steel bridges with multi-cracks. J VibroEng 19(6):4198–4209

Feng Q-M, Zhao L (2001) Buekling analysis of buried pipes subjected to fault movements. Earthq Eng Eng Vib 1(4):80–87

Gou HY, Shi XY, Zhou W, Cui K, Pu QH (2017) Dynamic performance of continuous railway bridges: numerical analyses and field tests. J Rail Rapid Transit, Proc Inst Mech Eng Part F. https://doi.org/10.1177/0954409717702019

Gou HY, Wang W, Shi XY, Pu QH, Kang R (2018) Behavior of steel-concrete composite cable anchorage system. Steel Compos Struct 26(1):115–123

Jiang T, Xu W-Y, Chen H, Lu J (2005) Numerical analysis of stability for rock mass in arch dam abutment impacted by fault and simulation of fault treatment. Chin J Rock Mech Eng 24:5840–5844

Jiang Z, Fu S, Li S, Hu D, Feng S (2007) High pressure permeability test on hydraulic tunnel with steep obliquity factor? Under high pressure. Chin J Rock Mech Eng 26(11):2318–2323

Liu Y (1987) The classification and evaluaton of active faults in engineering geology. J Xi Coll Geol 9(4):40–47

Liu X (2004) on rupture propagation of active faults in soil. Chin J Geotech Eng 26(3):425–427

Liu Z, Liu X (2003) Determination of tunnel fault by the method of fault parameter forecast. Chin J Rock Mech Eng 22(9):1547–1550

Prestininzi A, Romeo R (2000) Earthquake-induced ground failures in Italy. Eng Geol 58:387–397

Shi YL, Men YM, Liu Y, Chu C-M (2009) Research on the destruction mechanism of city overpass by ground fissure in xi and city and the controlling measures. J Earth Sci Environ 31(1):89–93

Wang C, Yang Y (2007) The elastic-visco displacement back analysis of Wushaoling tunnel F7 fault. J China Railway Soc 29(2):132–135

Wang T-N, Liu J-X, Yu Y-B (2009) Spatial dynamic analysis of isolated bridges subjected to near-fault ground motion. J Traffic Transport Eng 9(5):20–25

Yang CW, Zhang JJ, Wang ZZ, Hou JQ, Si CL (2018) Research on time-frequency analysis method of active earth pressure of rigid retaining wall subjected to earthquake, environmental earth sciences. https://doi.org/10.1007/s12665-018-7325-6

Zhang S, Xu J, Cao H (2001) Analysis of earthquake faulting on the destruction of the underground oil (gas) pipeline. Seismol Geol 23(3):432–438